Cement and Concrete Research 152 (2022) 106658

Contents lists available at ScienceDirect

Cement and Concrete Research

journal homepage: www.elsevier.com/locate/cemconres

A patchy particle model for C-S-H formation

Achutha Prabhu [a,*], Jorge S. Dolado [b,c], Eddie A.B. Koenders [d], Rafael Zarzuela [e], María J. Mosquera [e], Ines Garcia-Lodeiro [f], María Teresa Blanco-Varela [f]

[a] TECNALIA, Basque Research and Technology Alliance (BRTA), Building Technologies Division, Parque Tecnológico de Bizkaia, Astondo Bidea, Edificio 700, 48160 Derio, Spain
[b] Centro de Física de Materiales, Centro Mixto CSIC-UPV/EHU, Paseo Manuel Lardizabal 5, 20018 San Sebastián, Spain
[c] Donostia International Physics Center, Paseo Manuel Lardizabal 3, 20018 San Sebastián, Spain
[d] Institute of Construction and Building Materials, Technical University of Darmstadt, Franziska-Braun-Strasse 3, 64287 Darmstadt, Germany
[e] Department of Physical Chemistry, Faculty of Sciences, Universidad de Cádiz, Campus Río San Pedro s/n, 11510 Puerto Real, Cádiz, Spain
[f] Spanish National Research Council CSIC, Eduardo Torroja Institute for construction science (IETcc), Serrano Galvache 4, 28033 Madrid, Spain

ARTICLE INFO

Keywords:
Calcium-silicate-hydrate (C-S-H)
Cement
Simulations
Silicate polymerization

ABSTRACT

The composition and structure of Calcium-Silicate-Hydrate (C-S-H) phases depends on various reaction parameters leading to its formation. Molecular Dynamic simulation studies probing the formation and structure of C-S-H are generally computationally expensive and can reach only very short time scales. Herein, we propose a coarse graining approach to model the formation of C-S-H, using patchy particles and a modified Patchy Brownian Cluster Dynamics algorithm. The simulations show that patchy particle systems can recover the qualitative kinetic evolution of C-S-H formation, and the obtained final structures were comparable to previously reported molecular dynamics studies and experiments. The model was extended to study the effect of water in the polymerization of tetraethoxysilane oligomers, the principal component of an impregnation treatment for deteriorated concrete surfaces. The intermediate system properties predicted by the simulations, such as viscosity and gel time, and structure were found to be well in accordance with the tailored experiments.

1. Introduction

Concrete and Portland cement based materials are, the most commonly employed building materials for structural elements, façades, pavements, etc., since the late XIX century. These materials have a multi-scale structure and the origin of many of its properties are attributed to the Calcium-Silicate-Hydrate (C-S-H) gel [1–3]. C-S-H gel is the main cement hydration product and is formed by hydration of Alite (C_3S) and Belite (C_2S). It can occupy more than 60% of the total volume of hydration products and has a variable composition [4]. The structure of C-S-H gel has been a subject of investigation over the last few decades and has produced great advancements employing experimental tools such as NMR, microscopy etc. and also simulation studies [5], which we briefly explore in this work.

C-S-H is found to have a poorly crystalline structure at the molecular level and is often considered as having a defective tobermorite like structure. In simulation studies, two schools of thought can be encountered while investigating the structure of C-S-H. The first approach is to start with a tobermorite structure and to introduce defects to make it consistent with experimental observations [6,7], and the second approach is to follow the polymerization reaction of calcium and silica species, without imposing any structural constraints [8,9]. The latter approach is followed in the present study and hence will be given more focus. Studies on the defective tobermorite approach, following selective removal of bridging silicate and the addition of calcium species [7,10] were able to produce stable C-S-H structures. Recent works using defective building blocks model [11] have attained a better correspondence with many of the experimental observations for systems including calcium-aluminium-silicate-hydrates [12,13]. These findings have vastly helped in the refinement of thermodynamic modeling of C-S-H [14]. On the other hand, the early Molecular Dynamics (MD) simulations focusing on the kinetics of the sol-gel process and polymerization reactions leading to the formation of silicates go back to late 1990's [15]. Atomistic simulation studies on C-S-H formation from $Si(OH)_4$ and Ca

* Corresponding author.
E-mail addresses: achutha.prabhu@tecnalia.com (A. Prabhu), jorge_dolado002@ehu.eus (J.S. Dolado), koenders@wib.tu-darmstadt.de (E.A.B. Koenders), rafael.zarzuela@uca.es (R. Zarzuela), mariajesus.mosquera@uca.es (M.J. Mosquera), iglodeiro@ietcc.csic.es (I. Garcia-Lodeiro), blancomt@ietcc.csic.es (M.T. Blanco-Varela).

https://doi.org/10.1016/j.cemconres.2021.106658
Received 19 May 2021; Received in revised form 22 September 2021; Accepted 4 November 2021
Available online 25 November 2021

$(OH)_2$ have demonstrated the influence of composition on the reaction kinetics and resulting structures [8,9,16]. At lower Ca/Si ratios, the degree of polymerization of the silicate chain gets higher. At higher Ca/Si ratios, the structure of the resulting C-S-H gel is determined by the fastest reaction kinetics instead of the thermodynamic stability. Also, it has been noted that except at very low Ca/Si ratios, the formed silicate chains prefer linear structure, and the length of such linear chains can be described using a $3n - 1$ rule with n=1,2,3... [17].

Studies following microscopy techniques describe C-S-H to have a foil like and fiber like morphology [18], the formation of which was explored recently using computational simulations [19]. At nano scale, simulations have also showed the nano-branched [3] structure. In an attempt to grow C-S-H on calcite surfaces, ellipsoidal like structure [20] have also been observed. At micron scales, a foil like and long needle like appearance has also been observed (with width or thickness in nm range) [21]. Whether these structures evolve from a common starting point akin to the "bricks" in ref. [19] via difference in aggregation/organization is something that still needs further exploration.

In general, atomistic simulation approaches including MD simulations, need to include the thousands of water or solvent molecules. Even though most of these solvent molecules do not take part directly in the reaction of interest, their effect must be analyzed. Thus, the large number of atoms involved in MD simulations dramatically increases the computational cost, limiting the attainable simulation times to usually of the order of several pico seconds. A simpler model that can solve the above mentioned limitations, while retaining details of atomistic description to the extent possible is highly sought after.

In this context, coarse grained simulation approaches have gained a lot of interest in the past few decades, mainly to study complex biological systems such as proteins [22]. The so-called *patchy particle* based models have gained a lot of interest, since this approach allows simulating many complex systems using spheres interacting via directional forces [23]. Starting from relatively simpler Kern-Frenkel models [24] to complex systems varying in the number, shape and size of the patches have been developed [25] for increasing their similarity to the real world counterpart. Monte Carlo methods have been widely employed to study and discover the aggregation and phase behaviors of tetrahedral [26] and octahedral [27] patchy systems, and Wertheim theory based studies have been used to describe the structure [28,29]. As the previous studies focused on the structure rather than the kinetics, time dependent simulation methods are rarely employed. For modeling systems such as that of C-S-H, where the reaction is mainly kinetically driven, time dependent methods are preferred, given the objective is to study the kinetics and structure evolution. Patchy Brownian Cluster Dynamics (PBCD) is one such method and was able to successfully capture the kinetically driven polymerization reactions of two-patch particles [30]. Further, it was shown that the effect of solvent could be absorbed to simulation parameters, without resorting to the explicit representation as in atomistic MD simulations. Its non-patchy predecessor, Brownian Cluster Dynamics has been previously employed to study colloidal aggregation phenomena leading to sol-gel transition [31,32].

In the present work, PBCD is employed to model the reversible patchy aggregation of systems containing different amounts of tetrahedral and octahedral patchy particles, a simplified representation of the molecular species $Si(OH)_4$ and $Ca(OH)_2$. By adjusting the model and interaction parameters for a reference system, the model successfully replicated the kinetics and structure evolution of C-S-H gel over a wide range of Ca/Si ratios, and was verified by comparing with various reported atomistic MD simulations and experimental results.

Using the obtained parameters as a benchmark, the model was extended to study the effect of water content on the polymerization of a tetraethoxysilane (TEOS) oligomer, the main ingredient in an impregnation treatment for concrete [33]. Alkoxysilane based consolidation treatments have been used for rehabilitating deteriorated concrete surfaces due to their higher penetration capability and chemical compatibility with cementitious materials [34,35]. They polymerize spontaneously producing amorphous SiO_2 gels, which is compositionally similar to the siliceous aggregates, and their reticulation degrees and rigidity depends on the initial sol composition [36,37]. In the presence of cementitious matrix, they can produce C-S-H gel [38,39] or even incorporate into the already existing C-S-H phase [33], making them an ideal choice for rehabilitation purposes.

These impregnation treatments are highly influenced by the reaction conditions such as concrete type, state of decay, sol composition, Ca/Si ratios, water availability, reaction time/rate etc., which ultimately determine the mechanical properties and the overall effectiveness and durability of the treatment [40]. Predicting the behavior based solely on experimental studies is a challenging task due to the system complexity. For such complex systems, computational methods based on simplified models, like the present approach, can serve to predict the behavior and trends with respect to multiple variables, ultimately saving time and resources. Following a set of tailored experiments (rheology, gel time measurements, and MAS-^{29}Si NMR) of a given range of composition for calibration, simulation studies were carried out. Evolution of intermediate system compositions predicted by the simulations were found to be in good agreement with the experiments.

2. Model and methods

2.1. Simulation method

The atomistic species under consideration and their reaction were modeled using patchy particles and Patchy Brownian Cluster Dynamics (PBCD) algorithm. A detailed description of the basic patchy particle model and PBCD method can be found in ref. [30]. Here, only the key points and modifications are recalled. For a given hard sphere particle i with diameter d, patches are represented by surface decorations using circular patches with angular widths 2ω. The patch potential is modeled by restricting a square well potential to a given direction using a patch vector $\mathbf{v}_i^k$ (where k is the patch index for multi-patch systems starting from 1 to the number of patches), half opening angle ω and, relative interaction range of the square well potential ε_p and its depth u_p (see Fig. 1). The patchy pair potential for two particles i and j is given by

$$V\left(\mathbf{r}_{i,j}, \mathbf{v}_i^k, \mathbf{v}_j^k\right) = V_1\left(r_{i,j}\right) \cdot V_2\left(\hat{\mathbf{r}}_{i,j}, \hat{\mathbf{v}}_i^k, \hat{\mathbf{v}}_j^k\right), \text{for any } k \tag{1}$$

where $\mathbf{r}_{i,j}$ is the vector connecting the centers of the two particles, $\hat{\mathbf{r}}_{ij} = \mathbf{r}_{ij}/r_{ij}$ and $\hat{\mathbf{v}}_i^k = \mathbf{v}_i^k/v_i^k$. Further,

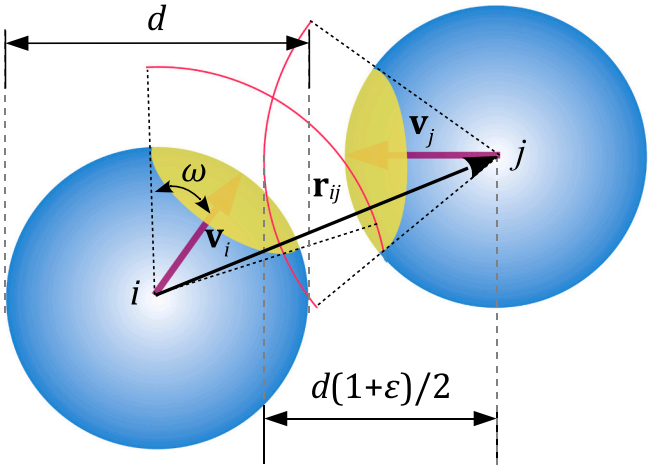

Fig. 1. A schematic showing the construction of patches and patchy interaction between two particles having one patch each. In this case, k in $\mathbf{v}_i^k$ is 1 for both particles and hence is omitted. (For interpretation of the references to color in this figure legend, the reader is referred to the web version of this article.)

$$V_1(r_{i,j}) = \begin{cases} \infty & r_{i,j} \le d \\ u_p & d < r_{i,j} \le d\cdot(1+\varepsilon_p) \\ 0 & r_{i,j} > d\cdot(1+\varepsilon_p) \end{cases} \quad (2)$$

and

$$V_2\left(\hat{\mathbf{r}}_{i,j}, \hat{\mathbf{v}}_i^k, \hat{\mathbf{v}}_j^k\right) = \begin{cases} 1 & \begin{cases} \hat{\mathbf{r}}_{i,j}\cdot\hat{\mathbf{v}}_i^k > cos(\omega), \text{for any } k \\ \text{and} \\ \hat{\mathbf{r}}_{j,i}\cdot\hat{\mathbf{v}}_j^k > cos(\omega), \text{for any } k \end{cases} \\ 0 & \text{otherwise} \end{cases} \quad (3)$$

Apart from the patchy potential, particles were also allowed to interact via an additional hard sphere square well potential similar to Eq. (2), with relative range ε and depth u_0.

The silica and calcium species are represented using four tetrahedrally placed patches and six octahedrally placed patches respectively (see Fig. 2 and explanation under simulation details subsection). The simulation starts at t_{sim}=0, with a given number of randomly positioned and oriented 4-patch (N_4) and 6-patch (N_6) particles in a cubic box of size L_{box} such that $N = N_4 + N_6$ and the total volume fraction occupied by particles is given by $\phi = N \cdot \pi \cdot d^3/{L_{box}}^3$. A simulation step is made of three following procedures in their respective order and is performed repeatedly in that order until the simulation is stopped.

Cluster formation: Particles are considered to be in contact when they are in interaction range (isotropic or patchy). In this step, particles in contact are bound with a probability $P = \alpha/(\alpha + \beta)$, where α is the probability of formation of a new bond and β is the probability of breaking an existing bond, and $0<(\alpha+\beta)<2$. The bond probability can be linked to the interaction potential using the relation $P = 1 - exp\left(\frac{u}{k_B\cdot T}\right)$, where $-u$ is the free energy per contact, k_B is the Boltzmann constant and T is the absolute temperature, and this relation holds for both patchy and isotropic interaction (see ref. [30]). At t_{sim}=0, bonds are formed using the combined probability P and later on new bonds are formed and existing bonds are broken using the probabilities α and β. The linking procedure results in the formation of three types of transient clusters when $P<1$ for both patchy and isotropic interaction. Clusters of particles in contact (satisfying all interaction criteria), but not necessarily bonded, clusters of particles bound only via isotropic interaction and finally, the clusters formed by particles bound by patchy bonds.

Movement: The movement procedure involves 2N times the random selection of a particle and attempt to perform an elementary translational or rotational motion with equal probability. At the end of the procedure, a particle in average is entitled to one translational and rotational step each. Translational step involves the attempt to move the selected particle in a random direction by a small Brownian displacement vector $\mathbf{s}_T$. The motion is accepted if the resultant motion does not lead to any overlap or bond rupture. Rotational motion is simulated by attempting to rotate the particle about a randomly selected axis passing through the center of the particle, by a small angle δ. The motion is accepted if the resultant operation does not break any existing bonds. Rotation of such a kind traces a maximum distance of ${s_R}^{max} = d \cdot \sin(\delta/2)$ for all points lying on the surface of the sphere contained by the plane passing through center of the sphere and perpendicular to the rotational axis. The distance traced at the points on the sphere surface where the axis passes is 0. The average distance traced by a point on the sphere surface can be calculated to be $s_R = \pi/4 \cdot {s_R}^{max}$. The elementary step sizes s_T and ${s_R}^{max}$ needs to be sufficiently small related to ε and ω such that the motion is Brownian.

Time increment: The cluster construction and movement procedures are followed by the increment of simulation time. Considering t to be the physical time, the relationships between t_{sim}, s_T and ${s_R}^{max}$ can be derived (see ref. [30] for details). The mean of squared displacement of a free particle at time step t_{sim} is then given by $\langle \mathbf{R}^2 \rangle = t_{sim} \cdot {s_T}^2$. If the physical time is defined as $t \equiv t_{sim} \cdot {s_T}^2$, we have $\langle \mathbf{R}^2(t) \rangle = 6 \cdot {D_1}^T \cdot t$, where ${D_1}^T$ is the translational diffusion coefficient of a free particle. The characteristic unit of time t_0 was defined as the time needed for a free particle to diffuse a distance equal to its squared diameter, which gives ${D_1}^T = d^2/(6 \cdot t_0)$. For short times, when ${D_1}^R \cdot t << 1$, where ${D_1}^R$ is the rotational diffusion coefficient, any patch vector $\mathbf{v}_i^k$ in average, performs a 2d random walk on the surface of the sphere $\langle (\mathbf{v}_i^k(t) - \mathbf{v}_i^k(0))^2 \rangle = v^2 \cdot 4 \cdot {D_1}^R \cdot t = t_{sim} \cdot {s_R}^2$. Combined with the diffusion equations $D_1^T = \frac{k_B \cdot T}{3 \cdot \pi \cdot \eta \cdot d}$, and $D_1^R = \frac{k_B \cdot T}{\pi \cdot \eta \cdot d^3}$, where η is the viscosity of the medium, we obtain the relation $s_T = \frac{s_R}{\sqrt{2}} = \frac{\pi \cdot {s_R}^{max}}{4 \cdot \sqrt{2}}$. Due to the inverse square relation between physical time and Brownian step size, there is a need for an optimum value for the step length in order to have a Brownian system that can reach higher physical time at reasonable computational expense. Previous studies have shown that for reasonable results within 10% of the real values, it is required to have $s_T/d < \varepsilon/5$ and $s_R/d < \omega/10$ [30,31,41]. In the present simulations, we employ s_T=0.008374 and ${s_R}^{max}$=0.0150, which falls well within the mentioned limits to avoid finite size effects.

2.2. Simulation details

The present simulations use a patchy particle model to represent the interactions between TEOS units and Portlandite units leading to the formation of C-S-H gel. All reactive species are considered as completely hydrolysed. A silicic acid unit can undergo self condensation

$$Si - OH + HO - Si \rightarrow Si - O - Si + H_2O \quad (4)$$

or can react with the Portlandite forming C-S-H gel, which can be represented by a generic simplified reaction

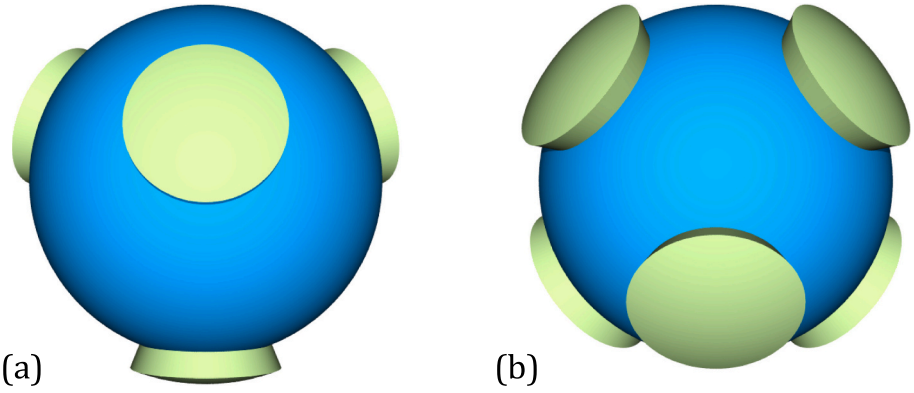

Fig. 2. A schematic showing (a) a tetrahedrally oriented 4-patch particle and (b) an octahedrally oriented 6-patch particle, with emphasis on the patchy interaction zone. (For interpretation of the references to color in this figure legend, the reader is referred to the web version of this article.)

$$Si(OH)_4 + Ca(OH)_2 \rightarrow C-S-H\ \ gel \quad (5)$$

In the present study, the $Si(OH)_4$ species is represented using a 4-patch spherical particle with tetrahedrally placed patches and the $Ca(OH)_2$ species is represented by a 6-patch particle with octahedrally placed patches (see Fig. 2 for a schematic). Thus, the reactions given in Eqs. (4) and (5) together can be simply represented by patchy bond formations between the two corresponding patchy particles. A patchy bond thus encompasses the atomistic details including bridging oxygen and the elimination of water molecule.

For simplicity, particle sizes and patch descriptions are kept the same for both species. Here, ω=0.4 rad and $\varepsilon = \varepsilon_p$=0.1 was chosen, which restricts the patches to be strictly monovalent by design. For a binary system containing both 4-patch and 6-patch particles, three kinds of patchy interactions/links are possible (4–4, 4–6, and 6–6), requiring the use of multiple patchy bond probabilities. The isotropic interaction between particles was assumed the same, irrespective of the interacting species. Essentially, the patchy bonds can be thought to represent highly local reactions of atomistic species, while the isotropic interaction can be thought of as originating from long range interactions, including solvent effects. The effect of solvents on step-growth polymerization has been demonstrated in a previous work [30].

Atomistic simulation studies have been carried out in an accelerated manner to reach larger time scales due to the slow nature of the condensation reactions [8,9]. In the present case, the bond probabilities and consequently a patchy bond formation collectively represent accelerated hydrolysis and condensation reaction. Thus, the patchy bond probabilities must be considered on an ad-hoc basis based on system constitution and the underlying reactions.

For the first set of benchmark simulations, the aim was to tune and calibrate the simulation parameters to match the reported MD simulation [8,9,16] and experimental [42,43] results. The system with N_6/N_4 or Ca/Si =1.4 was considered as a reference case. Random hard sphere (RHS) system with appropriate ϕ was generated for cell size L_{box}=20. The required number of randomly selected particles were set as 6-patch species and the rest were assumed as 4-patch species. Corresponding patch vectors were assigned to all particles without any preferential orientation. A small set of test simulations were run by varying the bond probabilities until the final structures were close to the ones described in literature. The resulting bond parameters, given in Table 1, were employed in the subsequent simulations. Once calibrated, various Ca/Si ratios were simulated by varying number of 4-patch (N_4) particles in the system, while keeping the 6-patch concentration a constant. Selected N_6/N_4 ratios ranged from 0.0 to 2.0 (see Table 2).

In the second set of simulations, effect of water in the polymerization of TEOS oligomers was studied. In line with the experimental data (see results section, Table 4), a system consisting of linear chains made of five 4-patch units with ϕ=0.27 was considered as the starting point. To generate the starting structure, an RHS system with ϕ=0.38 was considered with all particles having 4-patches. It was allowed to undergo irreversible patchy aggregation/polymerization (α_{4-4}=1,β_{4-4}=0 and without any isotropic interactions) under constraints. Only two patches out of the four could form patchy links (strictly linear polymerization) and the patchy cluster aggregation number was limited to 5, preventing the formation of larger chains. From the resulting simulation, the given number of pentamer chains corresponding to ϕ=0.27 were randomly selected. The generated system was relaxed for about 15 t_0, without allowing for new bond formations or bond rupture (α_{4-4}=0,β_{4-4}=0 and α_{iso}=0,β_{iso}=1). The resulting structure was used as the starting configuration for the simulations. The effect of water content was simulated by varying the isotropic bond probability.

Table 1
Details of the employed patchy ($x-y$) and isotropic bond probabilities.

Bond type ($x-y$)	α	β	P_{x-y}
4–4	1	0.0066	0.9934
4–6	1	0.0265	0.9742
6–6	1	0.1103	0.9000
Isotropic	1	0.3310	0.7513

Table 2
Details of the simulated systems.

N_6/N_4	N_4	N_6	N	ϕ
0.0	897	0	897	0.058770
0.7	898	629	1527	0.099942
1.0	898	898	1796	0.117548
1.4	897	1257	2154	0.140979
2.0	897	1796	2693	0.176256

2.3. Experimental details

In order to validate the capacity of the model to reproduce the polymerization of silicate species, a series of experiments were carried out using different TEOS oligomer-based sols. The sols were synthesized following a surfactant assisted route [44]. The systems in general varied in their initial viscosities, sol-gel transition times and water content.

The general synthesis process involves mixing the sol components under an ultrasound probe (Bandelin Ultrasonic HD3200) at a power of 1 W cm^{-3} during 10 min, so that the non-miscible components (silica precursor and water) can form a stable homogeneous emulsion [45,46].

The components of the sols were as follows: (1) A silica precursor (TES40 WN, Wacker Chemie AG) consisting of a pre-polymerized TEOS. According to the product technical data, TES40 WN is a liquid mixture of oligomeric ethoxysilanes, mainly linear chains, with an average length of five Si-O-Si units. (2) n-octylamine, which acts as a basic catalyst for the sol-gel process, and because of its surfactant properties, increases the miscibility of water with the oligomer. (3) De-ionized H_2O, which directly participates in the sol-gel reaction and was chosen as the composition variable. Table 3 shows the constitution of the different sols prepared for the study.

The viscosity of the sol was measured by using a concentric cylinder viscometer (DV-II+ with UL/Y adapter, Brookfield) at a constant temperature of 25 °C. Viscosity values were calculated as the slope of the shear stress vs shear rate curve in the linear regime (i.e. Newtonian behavior). In order to study the gelation process, 15 ml aliquots of the sols were cast into ϕ 8.7 cm Petri dishes and left in the open under room conditions (25 °C, 40% RH). The gel time of the sols was determined qualitatively by their rheology, assuming the endpoint as the moment where the viscosity sharply increases and the system stops flowing as a liquid (i.e. when the gel attains mechanical stability). For the sol with an intermediate H_2O proportion (0.5%), different replicates were prepared to measure the viscosity variations over time until gelation.

The initial and final structure of the systems after the sol-gel process was studied by analyzing ^{29}Si NMR of the formed xerogels after curing and drying for 28 d. Single-pulse (SP) MAS-^{29}Si NMR experiments were carried out on a Bruker ADVANCE WB400 spectrometer equipped with a multinuclear probe. Samples of powdered materials were packed in 4 zirconia rotors and spun at 8 kHz. Pulse length was 5 μs, with a recycle delay of 30 s and the number of transients was 8000.

Table 3
Composition of the sols, expressed as % volume, used for the experimental validation study of the silica precursor polymerization.

Sol	TES40	H_2O	n-octylamine
W0	99.84	0.00	0.16
W1	99.74	0.10	0.16
W25	99.59	0.25	0.16
W50	99.34	0.50	0.16
W100	98.84	1.00	0.16
W150	98.34	1.50	0.16

3. Results and discussion

3.1. Benchmark compared to MD results

In this section, the first set of simulations is compared with their MD simulation counterpart and reported experimental results. The compositions considered for the simulations were very similar to the ones employed in the previously reported simulation studies [8,9] for a better comparison. The first difference is in the number of reactive species in the sytem. Assuming a H_2O/SiO_2 molar ratio of 3, an equivalent MD system for Ca/Si ratio 2.0 should contain 25,126 atoms. In our model, the system simply has 2693 reactive species, which is about 10 times lower than the MD counterpart. The reduction of reactive species also reflects in the simulation time and efficiency. As a result, our model can access up to several microseconds in a reasonable amount of time.

Fig. 3 shows the large time configuration of the systems varying in Ca/Si ratios. It can be seen that as Ca/Si ratio increases, the extended silicate chain network in the resulting C-S-H structure breaks down. Also, the similarity of the final structures to the previous simulation results [9] is worth noting. Silicate reactions are usually characterized using the evolution of the connectivity Q_n, where n denotes the bridging oxygen atoms linked to a silicon atom. In the present case, Q_n is simply the number of 4-4 patchy links. Fig. 4 shows Q_n evolution as a function of time t/t_0. When the simulation starts, there are only Q_0 units present in the system. As the time passes, they form patchy links, giving rise to the other curves. At large times, they reach a plateau and no significant variation is observed thereafter.

It can be seen that depending on the Ca/Si ratios, the final Q_n values vary, with the lowest Ca/Si ratio case having higher degree of silicate chain polymerization (lowest Q_0). The presence of Ca species hinders the silicate chain growth and reduces the overall connectivity of the structure. This can be better visualized in Fig. 4. The terminating unit (Q_1) remains almost the same along the Ca/Si ratio range under consideration, while the higher Q_n curves decrease with the increase in Ca/Si ratio. This implies that the amount of cross-linking reduces with the incorporation of 6-patch species. It is known from experimental studies that linear structures are dominant in C-S-H gel [43]. To visualize this, the final fraction of crosslinks ($Q_3 + Q_4$) is plotted in Fig. 5. Data from the present simulations correctly recovers the behavior obtained from previous works, especially at higher Ca/Si ratios.

Another aspect that can be extracted from the Q_n analysis is the so called Q factor, which is simply given as $Q = Q_1/(Q_1 + Q_2 + Q_3)$ and is equal to twice the inverse of the mean silicate chain length. Fig. 5 shows the evolution of the Q factor as a function of Ca/Si ratio together with previous experimental and simulation results. The obtained data lie within the experimental observations and are almost identical to previous simulation results. This verifies that shorter silicate chains are preferred at higher Ca/Si ratios, consistent with previous observations.

In the present model, Brownian motion drives the system dynamics. It could be argued that Brownian diffusion is not entirely accurate for atoms. However, the patchy spheres are not single atoms, and it is known that when larger molecular clusters are formed, their diffusion becomes increasingly Brownian. Here, the implication of diffusion effects are lessened since larger cluster form even at early ages. The use of α_{x-y}=1 enhances the bond formation on first contact. This selection effectively accelerates the system kinetics and diminishes in part the effects originating from atomistic scales. This also implies that the time scale also needs to considered in a case by case manner with respect to common critical phenomena like gel time from experiments or simulations (this will be explored to some extent in the next section). While quantitative comparison can be made between the final states, only qualitative comparison is possible regarding the kinetics, unless the time is properly scaled. The takeaway message is that besides the mentioned shortcomings and simplifications, the model in general provides result corresponding to the previous observations.

3.2. Effect of water on the polymerization of a TEOS oligomer

A consolidation treatment based on TES40 WN was developed in a previous study for the surface treatment of deteriorated concrete structures [33]. Using TES40 WN as the silica source and Portlandite paste as the calcium source, the Q factor estimated from the ^{29}Si NMR data was ~ 0.57 for an estimated Ca/Si ratio ~ 0.74 (from solubility data) [33]. This value is consistent with the data given in Fig. 5, even though the reaction conditions and pathway are different. In this section, the polymerization reaction of same material is studied using the patchy particle model, and the effect of water content on polymerization is explored and compared with experimental results.

Table 4 shows the ^{29}Si NMR data for TES40 WN as obtained (fresh) and after storing in closed vessel for 2 months under laboratory conditions (aged). It can be seen that the aged sample has a slightly different structure from the fresh one implying that system evolves slowly by reacting with atmospheric moisture. Based on the obtained NMR data, and the possibility of slow system evolution, TES40 WN was assumed to consist mainly of linear pentamer units from the NMR data, given the mean chain length $=2 \cdot (Q_1 + Q_2 + Q_3)/Q_1$ was found to be ≈5. This assumption further limited the simulations to a single starting point, as explained in the simulation details.

The present experimental data on TEOS oligomer (TES40 WN) polymerization show that the gel time and initial viscosity of the system varies with water content. A time-resolved NMR experiment to study the polymerization kinetics was found to be largely unviable, as the NMR solvent could also interfere with the reactions. Table 5 shows the ^{29}Si NMR data of the xerogels obtained from a representative sample of sols given in Table 2, after 28 days.

In the simulations, specifically generated strictly linear pentamer chains are used to represent the TEOS oligomers (see simulation details section). As in the previous case, the system was considered to undergo an accelerated polymerization reaction, and therefore, the oligomers were considered as completely hydrolyzed. However, opposed to the monomer case, the experimental rates of the two reactions (hydrolysis and subsequent condensation) for each alkoxy group in the chain could

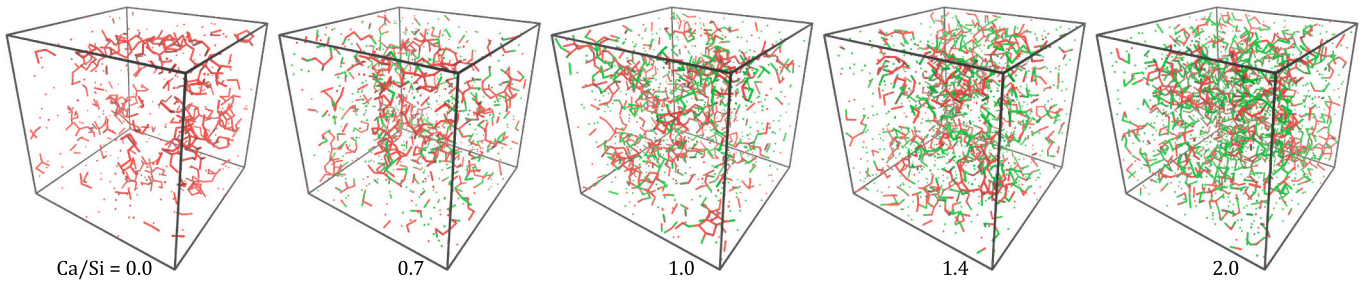

Fig. 3. Snapshots from simulations for various Ca/Si ratios, at t/t_0 ~ 23486. Small spheres indicate centres of particles and cylinders connecting them represent patchy links. Red and green colors denote 4-patch 6-patch particles respectively. Links follow a color scheme, where half of the cylinder is colored using the particle color to which it is linked to at that end. (For interpretation of the references to color in this figure legend, the reader is referred to the web version of this article.)

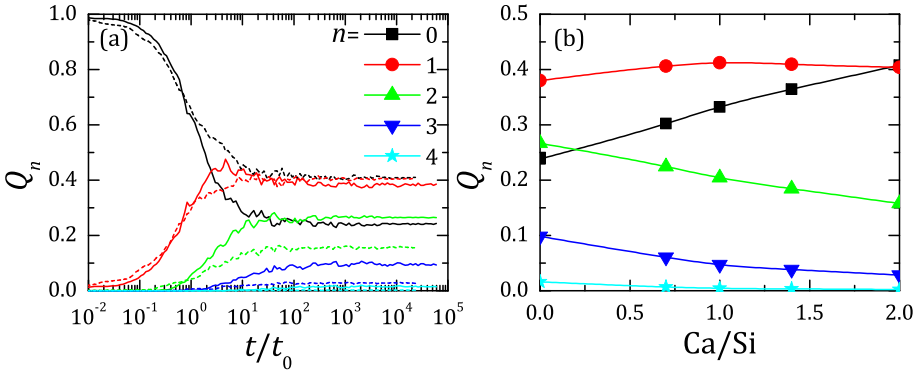

Fig. 4. (a) Obtained Q_n evolution based on the simulations based on Table 2. The solid curve represents N_6/N_4=0 and the broken curve represents N_6/N_4=2.0. (b) Final Q_n values obtained as a function of Ca/Si ratio, where the curves are guide to the eyes. Legend is common for both plots. (For interpretation of the references to color in this figure legend, the reader is referred to the web version of this article.)

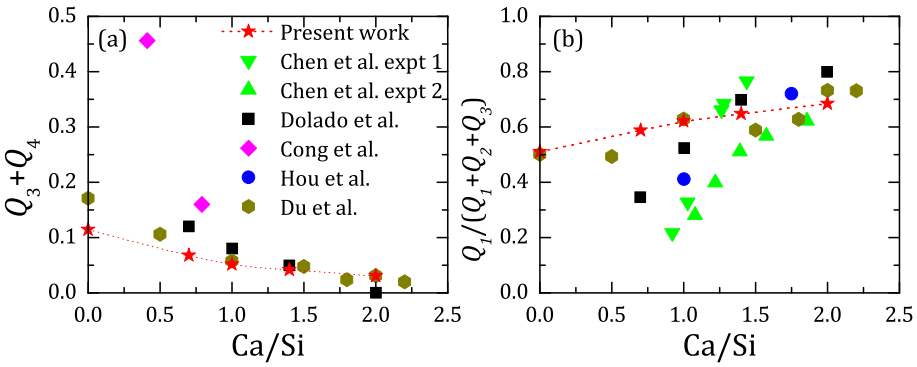

Fig. 5. Fraction of non-linear structures, measured using (a) the sum $Q_3 + Q_4$ and (b) the Q factor as a function of Ca/Si ratio. Results from present work are compared with the experimental data adapted from Chen et al. [42] and Cong et al. [43] and simulation data adapted from Dolado et al. [8], Du et al. [9] and Hou et al. [16]. Curves are guide to the eyes and both plots use a common legend. (For interpretation of the references to color in this figure legend, the reader is referred to the web version of this article.)

Table 4
MAS-^{29}Si NMR data (in fraction) of TES40 WN compared with the simulation model.

Sample	Q_0	Q_1	Q_2	Q_3	Q_4
Fresh	0.1020	0.3520	0.3870	0.1580	0.0010
Aged	0.0696	0.2879	0.3754	0.1101	0.1570

Table 5
MAS-^{29}Si NMR data (in fractions) of the obtained xerogels after 28, for some representative sols in Table 3.

Sol	%H_2O	Q_1	Q_2	Q_3	Q_4
W1	0.1	0.165	0.340	0.246	0.249
W50	0.5	0.034	0.125	0.384	0.458
W150	1.5	0.084	0.109	0.325	0.482

vary. Alkoxy groups undergo very slow hydrolysis at low H_2O content. However, the ambient moisture can interact with the system, resulting in an acceleration of the polymerization reaction. As the reaction is carried out in an open vessel, the formed reaction product (ethanol) can evaporate, which can also affect the reaction rate. In the simulations, the patchy interaction parameters were kept as before (see Table 1). The effect of water and the above mentioned effects were absorbed into the isotropic interaction potential (P_{iso}). With increasing P_{iso}, the particles stay together for longer times. They have more time to reorient and make patchy links, accelerating the polymerization reaction.

A series of simulations were carried out by varying P_{iso}. Fig. 6 shows the starting pentamer configuration and large time structures for a series of simulations varying in P_{iso}. It can be seen that P_{iso} plays an important role on the structure of the system, which was then analyzed in detail following the evolution of silicate connectivity. Fig. 7 shows the Q_n evolution of some representative cases. As P_{iso} increases, the isotropic and patchy interactions compete with each other and Q_n evolves

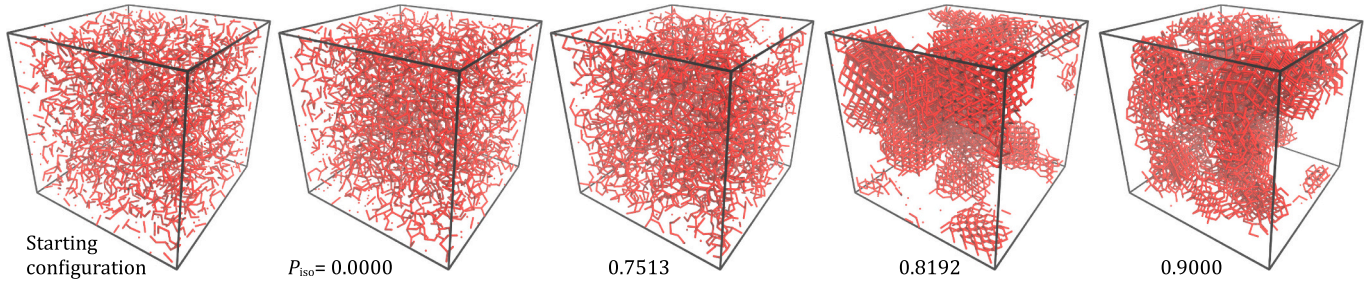

Fig. 6. Snapshots from simulations for various P_{iso}, at $t/t_0 \sim 6619$. Small spheres indicate centres of particles and cylinders connecting them represent patchy links. Links across box boundaries are not shown. (For interpretation of the references to color in this figure legend, the reader is referred to the web version of this article.)

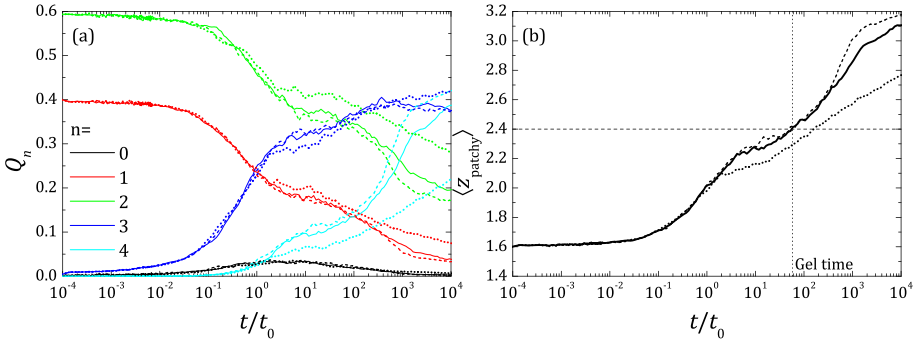

Fig. 7. (a) The Q_n evolution of the pentamer system with for different P_{iso} values. (b) Calculated patchy coordination number $\langle z_{patchy} \rangle$ evolution with time. Dotted curve corresponds to P_{iso}=0.872, solid curve corresponds to P_{iso}=0.9 and dashed curve corresponds to P_{iso}=0.9736. Method to estimate gel time for one case is also shown. (For interpretation of the references to color in this figure legend, the reader is referred to the web version of this article.)

differently for each case. For lower P_{iso} cases, Q_4 evolves rather slowly. Higher P_{iso} favours early isotropic aggregation, which in turn results in higher amount of cross-linking, as evidenced by the evolution of the Q_4 curves. Also, it can be seen that the Q_n curves are not stabilized, meaning that the system evolves slowly over long periods of time. Importantly, it is found that the large time Q_n values are in the range of the obtained experimental results in Table 5.

Polymerization can sometimes lead to the formation of gels. As seen from Fig. 6, percolation can occur in the system, but the obtained structures can be diverse. The systems with P_{iso}= 0.0 and 0.7513 have a random 3d network, while higher P_{iso} values lead to dense aggregated structures. In the simulations, gelation is usually represented by the formation of a percolating structure. However, percolation is simply a geometric phenomenon leading to a connectivity transition. It is the so called 'rigidity percolation' that needs to be considered while linking gelation in simulations to experiments. According to topological constraint theory, the average coordination number of the particles in system must be higher than 2.45 for it to be mechanically stable or rigidity percolation to occur [47]. Applying the principle to the patchy particle system, we can estimate the rigidity percolation (gelation) time (in terms of simulation time) by comparing the average patchy coordination numbers $\langle z_{patchy} \rangle$. Fig. 7 shows the estimation of simulation gel time by comparing $\langle z_{patchy} \rangle$ to the rigidity percolation threshold of 2.4. In Fig. 6, the first two resultant structures have $\langle z_{patchy} \rangle$<2.4 and the remaining have $\langle z_{patchy} \rangle$>2.4, while all four systems are geometrically percolating. Assuming the gel time as an identifying factor, simulation time may be rescaled for a better comparison among themselves or with experiments.

Following the identification of gel time, the simulation times were rescaled in an attempt to compare with the experiments. For this, the inverse of the mean square displacement (MSD or $\langle \mathbf{R}^2 \rangle$) of particles multiplied by the simulation time (or simply, the friction coefficient, which is proportional to the system viscosity) was used as a reference. On a first approximation, the rescaled P_{iso}=0.9 case was found to represent a water content of 0.05% in the experimental data, given that the system viscosity (here, the friction coefficient) at around 20 min and at gel time was close to the experimental observations (see Fig. 8a). It was assumed that this relation is valid and thus, similar comparisons could be made with other cases.

The data from a small number of simulated P_{iso} cases were rescaled using their gel times and were compared to experiments in a case by case manner. The comparisons implied a linear relation between water content and P_{iso} (Fig. 8b). It was also found that this relation also follows the correct Q_n evolution trends the with respect to water content. A scaling parameter for simulation gel time was calculated by comparing the water content and $P_{iso,}$ and experimental gel times. Using this scaling parameter, intermediate cases with varying water content could be simulated and their time frame scaled to match with the experimental counterpart. Following this method, the simulations were able to predict the gel times (Fig. 9a) and the initial viscosities (Fig. 9b) as a function of water content, within reasonable limits.

4. Conclusions

A new patchy particle based approach was introduced to model the reaction of molecular species using PBCD algorithm. The number of particles in the present system are reduced compared to traditional atomistic simulations because of two reasons. The use of patchy particle model effectively reduces the atomistic details and the reactive species were represented using judiciously placed patches. Further, the lack of physical representation of smaller entities like the solvent molecules also reduces a large number of particles in the simulations. The model effectively reduces the representation of many chemical reactions to a simply patchy link formation and the solvent effects etc. were absorbed

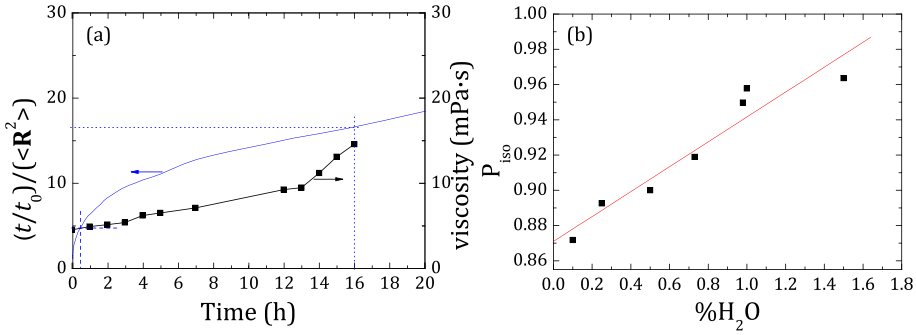

Fig. 8. (a) Time evolution of viscosity as measured by experiments for 0.05% water content and time evolution of friction coefficient of an average particle plotted against rescaled time. The dashed lines are guides to measure the early age and gel time friction coefficients. (b) P_{iso} plotted against water content. The red line is a linear fit. (For interpretation of the references to color in this figure legend, the reader is referred to the web version of this article.)

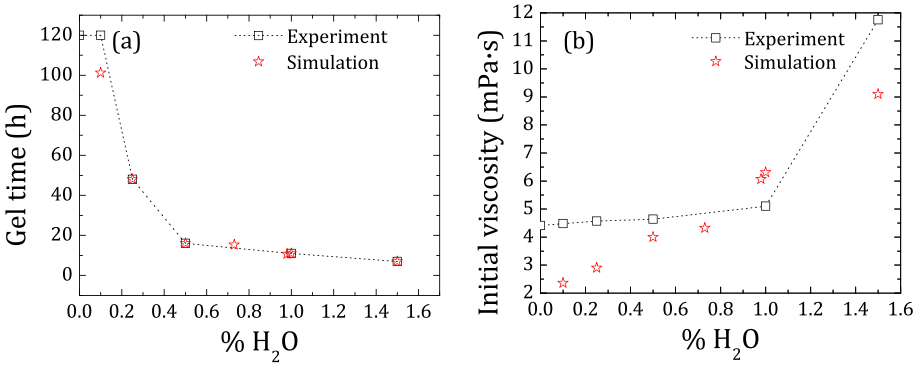

Fig. 9. (a) Gel time and (b) initial viscosity plotted against water content for the experimental and simulation data. (For interpretation of the references to color in this figure legend, the reader is referred to the web version of this article.)

in to the simulation parameters. This simplification has its consequences, as the interaction potentials of the patchy systems had to be adjusted each time for the system under consideration, based on the systems' chemical composition. In spite of the limitations, promising results were obtained.

To demonstrate the capabilities of the approach, formation of C-S-H gel having varying composition was studied using a system containing particles with tetrahedrally and octahedrally placed patches. The bond probabilities of the patchy particles were adjusted to appropriate values for the silicate system under consideration and to mimic previous simulation and experimental reference data on C-S-H formation via polymerization. A set of benchmark simulations were carried out using these parameters for C-S-H systems with a wide range of compositions. The extent of reaction, final structure and connectivity of silicate species were found to be in the range of data from reported experimental and simulation studies. The evolution of reaction kinetics, even though qualitative due to the simplifications of the system showed correct trends.

As a continuation, the effect of water on polymerization of TEOS based oligomer was modeled. In this case, the effect of water was absorbed in to the isotropic bond probability. Considering the experimental data, oligomer chains were modeled as linear pentamers of 4-patch particles. Systems with various amount of water were simulated. Using rigidity percolation as a reference, the simulation times were rescaled and results were compared with experimental data. Relations were elucidated between the simulation parameters and experiments, such that the system evolution at intermediate composition could be obtained from the simulations. As a result, gel times and viscosities were reproduced up to a reasonable degree. Even though the present study forms a first approach, the results indicate that more research in this direction could be of interest. The simulation predictions helped to understand the structural evolution of the polymerization reaction and synergistically aided in the development and fine-tuning of TEOS based consolidant materials by predicting the gel times and initial viscosity of several consolidant compositions under consideration.

In general, the PBCD model was extended to be capable of handling multiple reversible patches and mixed patch systems with varying interaction for each kind of patchy links. The potential of the model was shown by the study on two silicate based systems and results were found to be comparable with previous simulations and experiments. The model still has scope for improvement, like the use of different sized particles to represent the size differences of the interacting species instead of uniform ones [48]. The present approach opens up the door to study more complex cementitious systems such as the reaction between admixtures and cements using simplified representations. Further, patchy particle models seems to have a potential application to study the mesoscale structure of C-S-H, where the nucleation and growth leads to the observed foil like structures [19] and directional growths give rise to various growth patterns and morphology.

CRediT authorship contribution statement

Achutha Prabhu: Conceptualization, Software, Investigation, Writing - Original Draft Preparation.

Jorge S. Dolado: Conceptualization, Investigation, Writing - Original Draft Preparation.

Eddie A. B. Koenders: Supervision.

Rafael Zarzuela: Investigation, Writing - Original Draft Preparation.

María J. Mosquera: Investigation, Funding acquisition.

Ines Garcia-Lodeiro: Investigation, Resources.

María Teresa Blanco-Varela: Investigation, Resources.

All authors contributed equally to Writing - Review and Editing.

Declaration of competing interest

None.

Acknowledgements

The work described in this manuscript has been performed under InnovaConcrete EC project, supported by funding from the European Union's Horizon 2020 Research and Innovation Programme under Grant Agreement N° 760858. AP and JSD also acknowledge the support received from the BASKRETE initiative and the Joint Transborder Laboratory (LTC) “Aquitaine-Euskadi Network in Green Concrete and Cement-based Materials”.

References

[1] H.M. Jennings, J.W. Bullard, J.J. Thomas, J.E. Andrade, J.J. Chen, G.W. Scherer, Characterization and modeling of pores and surfaces in cement paste: correlations to processing and properties, J. Adv. Concr. Technol. 6 (1) (2008) 5–29, https://doi.org/10.3151/jact.6.5.

[2] E.A.B. Koenders, J.S. Dolado, K. van Breugel, A. Porro, URL, in: Nano to Microlevel Modeling of Cement-based Materials, Nanotechnology of Concrete: The Next Big Thing Is Small, ACI Special TechnicalPublication 267, 2009, pp. 1–10URL https://www.concrete.org/publications/internationalconcreteabstractsportal/m/details/id/51663278.

[3] J.S. Dolado, K. van Breugel, Recent advances in modeling for cementitious materials, Cem. Concr. Res. 41 (7) (2011) 711–726, https://doi.org/10.1016/j.cemconres.2011.03.014.

[4] H.F.W. Taylor, Cement Chemistry, Academic Press, London, 1990, https://doi.org/10.1680/cc.25929.

[5] A.J. Allen, J.J. Thomas, H.M. Jennings, Composition and density of nanoscale calcium-silicate-hydrate in cement, Nat. Mater. 6 (4) (2007) 311–316, https://doi.org/10.1038/nmat1871.

[6] X. Cong, R.J. Kirkpatrick, 29Si MAS NMR study of the structure of calcium silicate hydrate, Adv. Cem. Based Mater. 3 (3–4) (1996) 144–156, https://doi.org/10.1016/1065-7355(96)00023-5.

[7] A. Ayuela, J.S. Dolado, I. Campillo, Y.R. de Miguel, E. Erkizia, D. Sánchez-Portal, A. Rubio, A. Porro, P.M. Echenique, Silicate chain formation in the nanostructure of cement-based materials, J. Chem. Phys. 127 (16) (2007), 164710, https://doi.org/10.1063/1.2796171.

[8] J.S. Dolado, M. Griebel, J. Hamaekers, A molecular dynamic study of cementitious calcium silicate hydrate (C-S-H) gels, J. Am. Ceram. Soc. 90 (12) (2007) 3938–3942, https://doi.org/10.1111/j.1551-2916.2007.01984.x.

[9] R.J.-M. Pellenq, A. Kushima, R. Shahsavari, K.J. Van Vliet, M.J. Buehler, S. Yip, F.-J. Ulm, A realistic molecular model of cement hy drates, Proc. Natl. Acad. Sci. 106 (38) (2009) 16102–16107, https://doi.org/10.1073/pnas.0902180106.

[10] D. Hou, Molecular Simulation on Cement-based Materials: From Theory to Application, Springer, Singapore,Singapore, 2020, https://doi.org/10.1007/978-981-13-8711-1.

[11] G.W. Scherer, F. Bellmann, Kinetic analysis of C-S-H growth on calcite, Cem. Concr. Res. 103 (2018) 226–235, https://doi.org/10.1016/j.cemconres.2016.07.017.

[12] A. Ouzia, K. Scrivener, The needle model: a new model for the main hydration peak of alite, Cem. Concr. Res. (2018), https://doi.org/10.1016/j.cemconres.2018.08.005.

[13] G. Kovačević, B. Persson, L. Nicoleau, A. Nonat, V. Veryazov, Atomistic modeling of crystal structure of Ca1.67SiHx, Cem. Concr. Res. 67 (2015) 197–203, https://doi.org/10.1016/j.cemconres.2014.09.003.

[14] T. Du, H. Li, Q. Zhou, Z. Wang, G. Sant, J.V. Ryan, M. Bauchy, Chemical composition of calcium-silicate-hydrate gels: competition between kinetics and thermodynamics 3 (6) (2019), 065603, https://doi.org/10.1103/physrevmaterials.3.065603.

[15] G. Kovačević, L. Nicoleau, A. Nonat, V. Veryazov, Revised atomistic models of the crystal structure of C–S–H with high C/S ratio, Z. Phys. Chem. 230 (9) (2016) 1411–1424, https://doi.org/10.1515/zpch-2015-0718.

[16] A.K. Mohamed, S.C. Parker, P. Bowen, S. Galmarini, An atomistic building block description of C-S-H - towards a realistic C-S-H model, Cem. Concr. Res. 107 (2018) 221–235, https://doi.org/10.1016/j.cemconres.2018.01.007.

[17] A. Kumar, B.J. Walder, A.K. Mohamed, A. Hofstetter, B. Srinivasan, A.J. Rossini, K. Scrivener, L. Emsley, P. Bowen, The atomic-level structure of cementitious calcium silicate hydrate, J. Phys. Chem. C 121 (32) (2017) 17188–17196, https://doi.org/10.1021/acs.jpcc.7b02439.

[18] A.K. Mohamed, P. Moutzouri, P. Berruyer, B.J. Walder, J. Siramanont, M. Harris, M. Negroni, S.C. Galmarini, S.C. Parker, K.L. Scrivener, L. Emsley, P. Bowen, The atomic-level structure of cementitious calcium aluminate silicate hydrate, J. Am. Chem. Soc. 142 (25) (2020) 11060–11071, https://doi.org/10.1021/jacs.0c02988.

[19] D.A. Kulik, G.D. Miron, B. Lothenbach, A structurally-consistent CASH+ sublattice solid solution model for fully hydrated C-S-H phases: thermodynamic basis, methods, and Ca-Si-H_2O core sub-model, Cem. Concr. Res. 151 (2022) 106585, https://doi.org/10.1016/j.cemconres.2021.106585.

[20] K. Yamahara, K. Okazaki, Molecular dynamics simulation of the structural development in sol–gel process for silica systems, Fluid Phase Equilib. 144 (1–2) (1998) 449–459, https://doi.org/10.1016/s0378-3812(97)00289-6.

[21] D. Hou, H. Ma, Z. Li, Morphology of calcium silicate hydrate (C-S-H) gel: a molecular dynamic study, Adv. Cem. Res. 27 (3) (2015) 135–146, https://doi.org/10.1680/adcr.13.00079.

[22] E.T. Rodriguez, I.G. Richardson, L. Black, E. Boehm-Courjault, A. Nonat, J. Skibsted, Composition, silicate anion structure and morphology of calcium silicate hydrates (C-S-H) synthesised by silica-lime reaction and by controlled hydration of tricalcium silicate (c3s), Adv. Appl. Ceram. 114 (7) (2015) 362–371, https://doi.org/10.1179/1743676115y.0000000038.

[23] M.R. Andalibi, A. Kumar, B. Srinivasan, P. Bowen, K. Scrivener, C. Ludwig, A. Testino, On the mesoscale mechanism of synthetic calcium–silicate–hydrate precipitation: a population balance modeling approach, J. Mater. Chem. A 6 (2) (2018) 363–373, https://doi.org/10.1039/c7ta08784e.

[24] A.E. Hafner, J. Krausser, A. Šarić, Minimal coarse-grained models for molecular self-organisation in biology, Curr. Opin. Struct. Biol. 58 (2019) 43–52, https://doi.org/10.1016/j.sbi.2019.05.018.

[25] L. Rovigatti, J. Russo, F. Romano, How to simulate patchy particles 41 (5) (2018) 59, https://doi.org/10.1140/epje/i2018-11667-x.

[26] N. Kern, D. Frenkel, Fluid–fluid coexistence in colloidal systems with short-ranged strongly directional attraction, J. Chem. Phys. 118 (21) (2003) 9882–9889, https://doi.org/10.1063/1.1569473.

[27] N. Rolland, A.Y. Mehandzhiyski, M. Garg, M. Linares, I.V. Zozoulenko, New patchy particle model with anisotropic patches for molecular dynamics simulations: application to a coarse-grained model of cellulose nanocrystal, J. Chem. Theory Comput. 16 (6) (2020) 3699–3711, https://doi.org/10.1021/acs.jctc.0c00259.

[28] F. Romano, E. Sanz, F. Sciortino, Phase diagram of a tetrahedral patchy particle model for different interaction ranges, J. Chem. Phys. 132 (18) (2010), 184501, https://doi.org/10.1063/1.3393777.

[29] E.G. Noya, C. Vega, J.P.K. Doye, A.A. Louis, Phase diagram of model anisotropic particles with octahedral symmetry, J. Chem. Phys. 127 (5) (2007), 054501, https://doi.org/10.1063/1.2752155.

[30] J.M. Tavares, C.S. Dias, N.A.M. Araújo, M.M.T. da Gama, Dynamics of patchy particles in and out of equilibrium, J. Phys. Chem. B 122 (13) (2017) 3514–3518, https://doi.org/10.1021/acs.jpcb.7b10726.

[31] R. Fantoni, G. Pastore, Wertheim perturbation theory: thermodynamics and structure of patchy colloids, Mol. Phys. 113 (17–18) (2015) 2593–2607, https://doi.org/10.1080/00268976.2015.1061150.

[32] A. Prabhu, S.B. Babu, J.S. Dolado, J.-C. Gimel, Brownian cluster dynamics with short range patchy interactions: its application to polymers and step-growth polymerization, J. Chem. Phys. 141 (2) (2014), https://doi.org/10.1063/1.4886585.

[33] M. Rottereau, J.-C. Gimel, T. Nicolai, D. Durand, Influence of the brownian step size in off-lattice Monte Carlo simulations of irreversible particle aggregation, Eur. Phys. J. E 18 (1) (2005) 15–19, https://doi.org/10.1140/epje/i2005-10027-5.

[34] S. Babu, J.-C. Gimel, T. Nicolai, C. De Michele, The influence of bond rigidity and cluster diffusion on the self-diffusion of hard spheres with square well interaction, J. Chem. Phys. 128 (20) (2008), https://doi.org/10.1063/1.2925686.

[35] R. Zarzuela, M. Luna, L.M. Carrascosa, M.P. Yeste, I. Garcia-Lodeiro, M.T. Blanco-Varela, M.A. Cauqui, J.M. Rodríguez-Izquierdo, M.J. Mosquera, Producing C-S-H gel by reaction between silica oligomers and portlandite: a promising approach to repair cementitious materials, Cem. Concr. Res. 130 (2020), 106008, https://doi.org/10.1016/j.cemconres.2020.106008.

[36] Y. Cai, P. Hou, C. Duan, R. Zhang, Z. Zhou, X. Cheng, S. Shah, The use of tetraethyl orthosilicate silane (TEOS) for surface-treatment of hardened cement-based materials: a comparison study with normal treatment agents, Constr. Build. Mater. 117 (2016) 144–151, https://doi.org/10.1016/j.conbuildmat.2016.05.028.

[37] E. Franzoni, B. Pigino, C. Pistolesi, Ethyl silicate for surface protection of concrete: performance in comparison with other inorganic surface treatments, Cem. Concr. Compos. 44 (2013) 69–76, https://doi.org/10.1016/j.cemconcomp.2013.05.008.

[38] M. Peeters, T. Bernards, M.V. Bommel, ^{17}O-NMR of sol-gel processes of TEOS and TMOS, J. Sol-Gel Sci. Technol. 13 (1/3) (1998) 71–74, https://doi.org/10.1023/a:1008699104854.

[39] A. Depla, D. Lesthaeghe, T.S. van Erp, A. Aerts, K. Houthoofd, F. Fan, C. Li, V. V. Speybroeck, M. Waroquier, C.E.A. Kirschhock, J.A. Martens, J. Phys. Chem. C 115 (9) (2011) 3562–3571, https://doi.org/10.1021/jp109901v.

[40] F. Sandrolini, E. Franzoni, B. Pigino, Ethyl silicate for surface treatment of concrete – part i: pozzolanic effect of ethyl silicate, Cem. Concr. Compos. 34 (3) (2012) 306–312, https://doi.org/10.1016/j.cemconcomp.2011.12.003.

[41] A. Barberena-Fernández, P. Carmona-Quiroga, M. Blanco-Varela, Interaction of TEOS with cementitious materials: chemical and physical effects, Cem. Concr. Compos. 55 (2015) 145–152, https://doi.org/10.1016/j.cemconcomp.2014.09.010.

[42] Z. Zhang, G.W. Scherer, A. Bauer, Morphology of cementitious material during early hydration, Cem. Concr. Res. 107 (2018) 85–100, https://doi.org/10.1016/j.cemconres.2018.02.004.

[43] S. Babu, J.-C. Gimel, T. Nicolai, Phase separation and percolation of reversibly aggregating spheres with a square-well attraction potential, J. Chem. Phys. 125 (19) (2006), 84512–10, https://doi.org/10.1063/1.2378832.

[44] J.J. Chen, J.J. Thomas, H.F. Taylor, H.M. Jennings, Solubility and structure of calcium silicate hydrate, Cem. Concr. Res. 34 (9) (2004) 1499–1519, https://doi.org/10.1016/j.cemconres.2004.04.034.

[45] M.J.Mosquera Diaz, J.F.Illescas Salinas, D.S.Facio Silva, Product for protecting and restoring rocks and other construction materials. https://patentscope.wipo.int/search/es/detail.jsf?docId=WO2013121058, 2013.

[46] D.S. Facio, M. Luna, M.J. Mosquera, Facile preparation of mesoporous silica monoliths by an inverse micelle mechanism, Microporous Mesoporous Mater. 247 (2017) 166–176, https://doi.org/10.1016/j.micromeso.2017.03.041.

[47] D.S. Facio, L.A.M. Carrascosa, M.J. Mosquera, Producing lasting amphiphobic building surfaces with self-cleaning properties, Nanotechnology 28 (26) (2017), 265601, https://doi.org/10.1088/1361-6528/aa73a3.

[48] J. Mauro, Topological constraint theory of glass 90 (2011) 31–37.